J. Fluid Mech. (2008), *vol.* 606, *pp.* 51–73.
doi:10.1017/S0022112008001729 Printed in the United Kingdom

Experiments on turbulent convection over a rotating continental shelf–slope

H. LIANG, R. C. HIGGINSON AND T. MAXWORTHY

Department of Aerospace and Mechanical Engineering, University of Southern California, CA 90089, USA

(Received 25 March 2007 and in revised form 14 March 2008)

A series of Southern Hemisphere experiments have been performed to study turbulent convection on a continental shelf–slope placed in a large rotating tank filled with fresh water. Dense salt water was uniformly released at the fluid surface above the shelf. The resulting negatively buoyant bottom flow travelled over the shelf and then downslope. The non-dimensional reduced gravity of the dense downslope flow was found to scale as $G' = g'h^{4/3}/(B_0^{2/3}W)$ for a fixed slope angle, where B_0 the buoyancy flux at the surface, g' the reduced gravity of the bottom flow, h the water depth above the shelf and W the width of the dense water source. Under rotation, a bottom Ekman layer, with superimposed roll waves, propagated down the slope and towards the left sidewall when looking down the slope. As the modified natural Rossby number P decreased, where $P = (B_0/f^3h^2)^{1/2}W/h$ and f is the Coriolis parameter, the appearance of the bottom layer had four different forms: laminar flow, the continuous formation of waves, the periodic release of wave groups, and the periodic generation of eddies. Vortices generated on the surface were cyclonic, suggesting, but not proving, that eddies in the dense bottom layer as originally formed were anticyclonic.

With a canyon cut from the middle of the shelf to the bottom of the slope, G' values measured in dense flows to the left of the canyon, were significantly reduced. The canyon channelled a large amount of dense fluid with a buoyancy considerably larger than that of dense flows on the slope. However, the flow regime criteria remained basically unchanged with eddies and downslope Ekman layer being able to partially cross the canyon.

1. Introduction

The experimental investigation reported here considers convection, produced by a negative buoyancy flux, above a combined shelf–slope in a rotating fluid. In many partially enclosed bodies of water, convection, due to a negative buoyancy flux at the free surface, can drive a mean flow through the system (see e.g. Maxworthy 1997 for a review). Negative buoyancy fluxes can arise through evaporation or the action of cold winds which cause surface cooling and freezing. Gill (1973) has suggested that buoyancy fluxes large enough to affect the overall dynamics of the oceanic system can be created by the high-salinity flows caused by salt rejection through freezing. In many natural systems the resulting convectively driven flows are also influenced by the Earth's rotation, so that products from convective mixing are influenced and diverted by the Coriolis force.

The present work is intended to model the combined effects of convection and rotation, that occur in the polar seas, with a focus on the Ross and Weddell Sea

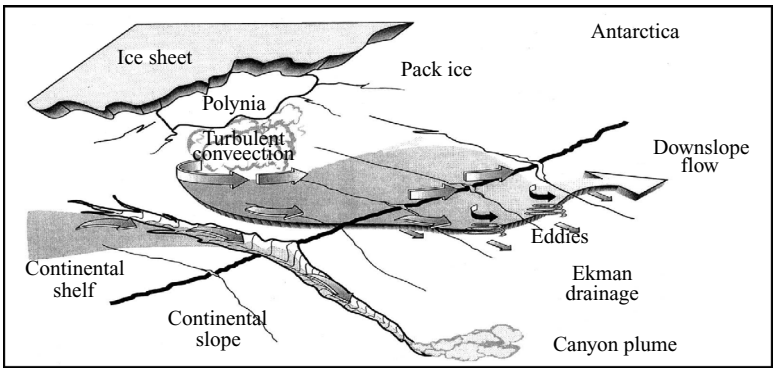

FIGURE 1. A schematic diagram of localized dense water production and resulting flow over the combined continental shelf–slope (Baines & Condie 1998, reproduced with permission).

in the Antarctic (Gordon *et al.* 1993; Gascard 1991; Gill 1973; AGU Antarctic Research Series volume 75). An aspect of particular interest to this problem is the convection that takes place in continental shelf regions, where reduced depths (300–500 m) can result in high-density products of convection. The dense water produced over continental shelves then descends to depths greater than 10^3 m down and along continental slopes. Thus the behaviour of the dense flow, under the influences of gravity and rotation down a sloping geometry, is of great oceanographic interest. A schematic diagram of such flows in nature can be found in the review by Baines & Condie (1998) (here figure 1). This figure shows localized dense water production over the shelf beneath a polyna, formation and convection of a dense plume, its motion along the shelf, and its descent down the slope as a sheet with eddy formation and Ekman drainage, or via a plume in a submarine canyon.

The present experiment used a similar rotating tank set-up to the experiments by Maxworthy & Narimousa (1994) and Jacobs & Ivey (1998), with the major difference that a plane slope with side boundaries was used rather than a flat surface or a truncated cone. The direction of rotation was clockwise, when viewed from above, which is consistent with natural flows in the Southern Hemisphere (Gordon *et al.* 1993; Muench & Gordon 1995; Gordon 1998). The presence of the boundaries was found to have a profound effect on the flow along the whole length of the slope, and given that many natural flows will be bounded on one or more sides (see e.g. Maxworthy 1997) a laterally restricted geometry was studied here. A plane slope geometry has also been considered in experiments by Lane-Serff & Baines (1998), Cenedese *et al.* (2004), and Etling *et al.* (2000). However, their investigations did not consider a convective source of dense fluid, but instead a continuous, localized, and relatively small source of fluid of known density was supplied to the slope. This meant that the density of the fluid onto the slope was fixed rather than being set by convective processes, as it would in the natural flows modelled here. The convection was initiated here using a dense fluid source which was placed above the shelf and covered half or all of the shelf area. This source was then supplied with a near-saturated salt solution.

Topographic variations, e.g. submarine canyons, can contribute substantially to the local down-slope flow by channelling the fluid into them (Baines & Condie 1998). The effect of such a canyon has been introduced into the present investigations. If we take, for example, the Weddell Sea, a number of wide canyons are known to extend from the 500 m deep Western Shelf to 4000 m, such as the Fedorov, Uruguary, Antarctic, Endurance, St. Martin and Aurora canyons (AGU Antarctic Research Series

volume 75). To model this, a series of experiments were performed with a canyon cut from the middle of the shelf to the bottom of the slope.

In what follows, two existing scaling laws for the buoyancy of the outflow from the shelf, produced by convection, are compared for bottom flows. The propagation and flow regimes for both bottom boundary layers and surface fresh water are studied, under different rotation rates, water depths and dense source flow rates and widths.

A description of the experimental apparatus and procedure is given in § 2. This is followed by a discussion of the present results on a continental shelf/slope, first in a non-rotating fluid, in § 3.1, to provide a comparison for the results with rotation, presented in § 3.2. Flow morphology and eddy production are discussed in § 3.3 and § 3.4. Section § 4 contains investigations of the effect of the addition of a submarine canyon, in a non-rotating fluid and in a rotating fluid. The results are discussed in § 5.

2. Experimental procedure

The present experiments were designed to model the formation and descent of dense water such as that occurring at several locations around the Arctic and Antarctic continents. A clear acrylic tank with a rectangular base 120.5 cm × 89 cm was placed at the centre of a turntable of diameter 160 cm (figure 2). The shelf–slope configurations found at positions along the Antarctic coast, were represented by a horizontal shelf ($L \times W = 120.5\,\text{cm} \times 31\,\text{cm}$, see figure 2) placed along one of the longer sides of the tank and an adjacent slope placed at $\alpha = 15^\circ$ to the horizontal. The slope was fixed to the inward edge of the shelf, forming a constant slope to the tank floor (which was 16.5 cm vertically below the shelf). The tank was filled with fresh water to a prescribed depth, giving different values of h, the depth of the water above the shelf, in the range $1\,\text{cm} < h < 3.5\,\text{cm}$.

Convection was generated by supplying almost saturated salt solution to the surface of the fluid directly above the shelf. Large salt concentrations were used so that high buoyancy fluxes could be obtained while keeping the volume flux of source fluid to a minimum. A spatially uniform buoyancy flux was achieved by dripping the salt solution through porous hoses onto the bottom of a set of porous steel trays, in contact with the free surface of the fresh water, similar to those used in the convection experiments of Grimm & Maxworthy (1999). The trays contained layers of paper towel, which distributed the saline solution more evenly. Precision flow meters supplied a prescribed flux of the source fluid to the trays. Dye was added to the source fluid, allowing the structure of the dense flow downslope to be observed. The buoyancy flux B_0 at the surface, directly above the shelf, was calculated using

$$B_0 = \frac{Q_s g_s'}{A_S}\ (\text{cm}^2\text{s}^{-3}) \tag{2.1}$$

where Q_s is the volume flux of the salt solution (of density ρ_s) supplied to the area $A_S = L \times W$ directly above the shelf, $L = 120.5$ cm is the length and $W = 15.5$ or 31 cm is the width of the source, $g_s' = g(\rho_s - \rho_0)/\rho_0$ is the reduced gravity of the salt solution, g is the acceleration due to gravity, and ρ_0 is the density of fresh water. For future use the buoyancy input per unit length (L) of the source is defined as $B = Q_s g_s'/L = B_0 W$.

For experiments in a rotating fluid, after filling the tank with fresh water, it was allowed to 'spin-up' for approximately 30 minutes, before the buoyancy source was activated. The direction of the rotation was clockwise when viewed from above, in keeping with natural flows in the Southern Hemisphere. Unlike the schematic diagram

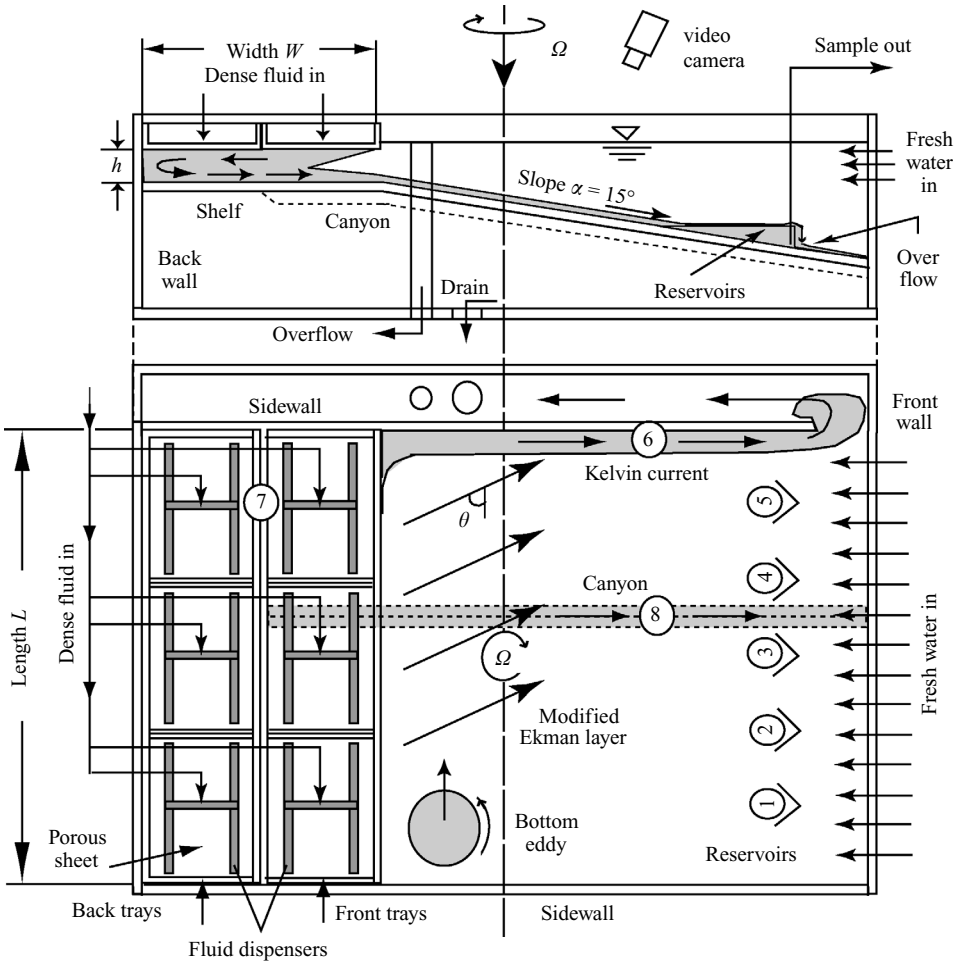

FIGURE 2. Side and plan views of the experimental tank. The tank has a horizontal shelf at the left-hand side of the sketch and a constant slope with the bottom end of the slope at the right-hand side of the sketch. Six removable trays with horizontal porous bottoms were placed on the water surface and covering half or all of the flat shelf. Density was measured at locations marked 1–8, with 1–5 in downslope catch basins, 6 in the Kelvin current, 7 on the middle of the shelf close to the left sidewall and 8 in the downslope canyon.

(figure 1), owing to sidewall effects, a dense current, called a Kelvin current in what follows, formed along the left-hand sidewall of the tank when looking down the slope (figure 2), and carried a modest fraction of the total outflow from under the shelf.

A range of rotation rates was studied in the present experiments, corresponding to values of the Coriolis parameter, $f = 2\Omega$, in the range of 0–0.87 s^{-1}, where Ω is the angular rotation rate. In both the rotating and non-rotating experiments the dense flow down the slope had a thickness of the order of 1–2 mm. To measure the density of this flow, five 'V'-shaped catchment reservoirs were placed approximately two thirds of the way down the slope, i.e. 40.6 cm from the edge of the shelf, and placed 20.3 cm apart along a line of constant depth. These are labelled '1–5' in figure 2. The fluid collected from these reservoirs (through hollow needles taped at the bottom) allowed the density of the dense layer to be measured with virtually no contamination by

fresh ambient fluid. Fluid was collected slowly, at the rate of 1 droplet every 1–3 s, and there was always an overflow from these reservoirs. Two other hollow needles, marked 6 and 7 in figure 2, were taped to the bottom, one 20.3 cm away from the shelf–slope edge and near the left wall, and the other one in the middle of the shelf and 15.2 cm from the left wall. Density measurements were made by taking a precise volume in a gravity bottle and weighing it using an electronic scale. This method gave fluid densities accurate to 0.00005 g cm^{-3}.

To avoid an accumulation of the dense fluid at the bottom of the slope during the experiments, a drain on the floor of the tank continuously removed the dense outflow. This fluid was replaced by fresh water from a distributed source placed just below the free surface on the opposite side of the tank to the buoyancy source. The relative positions of the fresh water source and dense fluid drain can be seen in figure 2. Constant fluid depth was maintained using an overflow pipe located next to the dense fluid drain.

In later experiments, a 90° triangular canyon was cut between reservoirs 3 and 4, from the middle of the shelf to the bottom of the slope (see figure 2). The start of the canyon at the middle of the shelf and the transition at the shelf–slope edge were smoothed to avoid turbulence generation around sharp edges. The canyon had an average width of 4.1 cm and depth of 2.1 cm. A tiny needle and suction tube were placed at the bottom of the canyon, a distance of 30.5 cm down from the shelf–slope edge, marked 8 in figure 2.

3. Convection onto a continent shelf–slope model

3.1. *Non-rotating ambient*

In this section the results of the experiments with no rotation ($f = 0\,\mathrm{s}^{-1}$) will be presented. Measurements of the density and flow morphology of the downslope flow are compared to existing theories and earlier observations.

At the start of these experiments, the flow of salt solution to the buoyancy source was switched on, and dense fluid was observed to descend, almost evenly, beneath the buoyancy source. The resulting convection beneath the source quickly became turbulent and mixed fluid began to flow down the slope, made visible by the addition of dye to the dense salt solution. A mean exchange flow under the source was set up with the dense fluid (see figure 2, side view), flowing down the slope, being replaced by fresh water entering from above.

The reduced gravity g', relative to the fresh water ambient, of the dense downslope flow was measured using a conductivity probe placed in one large capture reservoir on the middle slope. It is plotted as a function of time t in figure 3. The values of g' in the figure have been made non-dimensional following Phillips (1966), thus $g'h/(B_0W)^{2/3}$, and this appears to collapse the data; here $W = 31$ cm was the width of the buoyancy source. Similarly, time has been non-dimensionalized by $S/(B_0W)^{1/3}$, where $S = 45$ cm is the distance down the slope where the density was measured. However, it is shown below that this non-dimensionalization is not unique. In figure 3 a sudden increase in g' can be seen as the dense downslope flow reached the probe, which suggests that this layer initially formed a sharp density front. This is consistent with the dye observation. It may also be seen from the figure that a steady state was reached after a non-dimensional time of 2–3, after which g' remained approximately constant.

The downslope bottom flow remained quasi-steady and laminar for all non-rotating cases in the present experiments. Samples of the thin and dense downslope layer were

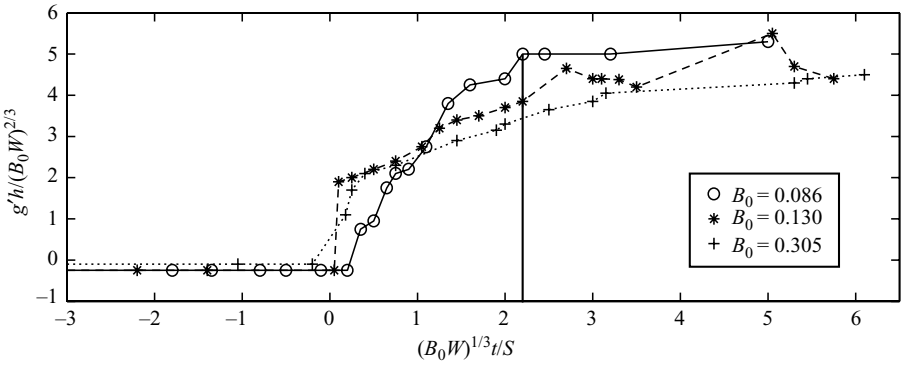

FIGURE 3. Conductivity probe measurements of the reduced gravity of the dense flow for three non-rotating experiments as a function of time. The three sets of data were obtained from experiments with different values of B_0, but all had $h = 2.2$ cm and $W = 31$ cm. The reduced gravity has been non-dimensionalized by $(B_0W)^{2/3}/h$, and time non-dimensionalized by $S/(B_0W)^{1/3}$, where $S = 45$ cm is the distance down the slope where the density was measured. The instant $t = 0$ coincides with the moment that the dense fluid first reached the conductivity probe.

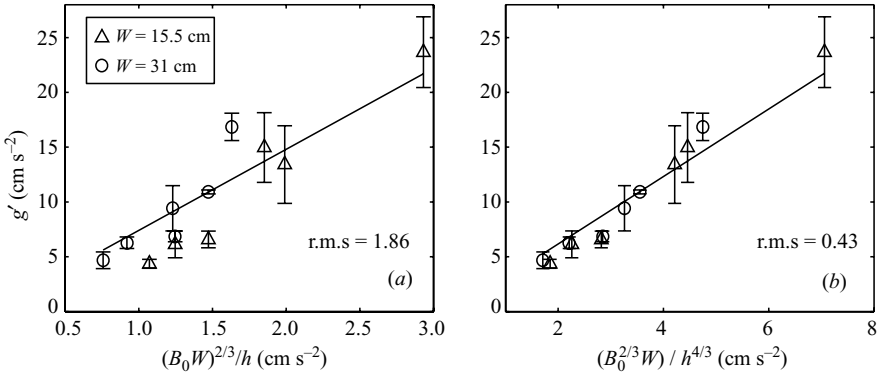

FIGURE 4. The reduced gravity g' of the dense downslope flow is plotted against the independent quantities (*a*) $g' = (7.40 \pm 1.86)(B_0W)^{2/3}/h$ proposed by Phillips (1966) and (*b*) $g' = (3.08 \pm 0.43)B_0^{2/3}W/h^{4/3}$ proposed by Maxworthy (1997). Each data point shows the mean value of g' measured at reservoirs 1 to 5, with the error bars showing the maximum and minimum values observed. The solid line in (*a*) is a lest-square fit of the form (3.1) and that in (*b*) shows (3.4). It is noted that the root-mean-square error of the linear least-square fit to the Maxworthy (1997) model is approximately a quarter that for the Phillips (1966) model.

captured in five reservoirs (see figure 2), and their density was measured. Samples were collected after the downslope flow became steady, typically about 30 min after the release of dense source into the porous pans. It took about 15–20 min for collection of a suitable sample by slowly withdrawing the bottom fluid from the catch basins.

The steady-state values of g' for a collection of experiments performed over a range of values of B_0, h and $W = 15.5$ or 31 cm are plotted in figure 4. The error bars show the maximum difference between the values of g' measured at reservoirs 1–5. It is likely that these errors are as a result of slight non-uniformity of the buoyancy source, however some of the spread may also be due to non-uniformity in the source of fresh fluid (see figure 2) setting up a systematic flow.

In figure 4(*a*) the measured values of g' have been plotted against the independent quantity, $(B_0W)^{2/3}/h$, which appears to collapse the data reasonably well. The solid line shows a linear least-square-root fit to the data and is of the form

$$g' = (7.40 \pm 1.86)\frac{(B_0W)^{2/3}}{h}. \tag{3.1}$$

This scaling for g' is in accordance with a model proposed by Phillips (1966). In this model Phillips, using dimensional analysis and buoyancy conservation, wrote down scalings for the buoyancy, g', and velocity, U, in a two-dimensional convective system closed at one end and fed by a surface buoyancy flux. Applying this model to the present case:

$$g' = \frac{(B_0W)^{2/3}}{h}F_1(z/h), \qquad U = (B_0W)^{1/3}F_2(z/h) \tag{3.2}$$

where W is the source width. Since in the present experiments g' was always measured as the average of the density of the fluid in the thin bottom layer, F_1 and F_2 will be constants. With F_1 set equal to a constant, (3.2) reduces to the relationship given by (3.1). Phillips applied (3.2) to field data obtained in the Red Sea, and showed that it provided a good model for the data.

More recently, however, Maxworthy (1996, 1997) has proposed an alternative model for convectively driven mean flow in a partially enclosed system. Based on observations of convection in a long channel, closed at one end and having the opposite end open but with a hydraulic control condition (Maxworthy 1996, 1997; Grimm & Maxworthy 1999), a three-layer model was suggested. In this model, two active upper fluid layers overlayed an, essentially passive, third lower layer. When a negative buoyancy flux was applied to the free surface, the two active layers flowed in opposite directions, with the top layer flowing towards the close end of the channel and the layer below moving towards the open, hydraulically controlled end. As the top layer moved towards the closed end it became progressively more dense, owing to the surface buoyancy flux, until it reached the closed end where the density closely matched that of the lower layer. At this location the fluid in the top layer descended and mixed, to feed the lower layer. Experiments by Grimm & Maxworthy (1999) have confirmed that there was negligible mixing between the layers over much of the length of the channel, except in the vicinity of the closed end. Thus, in addition to making use of the continuity of buoyancy, as done by Phillips (1966), the observation was made that in many cases buoyancy and convective terms in the vorticity equation are not necessarily of the same order, and instead a hydraulic control condition was applied at the open end. This condition takes the form of a constant composite Froude number, similar to that used in standard hydraulics for a single fluid layer. Studies of such composite flows include those of Armi (1986), Farmer & Armi (1986) and Lawrence (1990). Using these constraints, one obtains

$$g' = \frac{B_0^{2/3}W}{h^{4/3}}F_3(z/h), \; U = (B_0W)^{1/3}F_4(z/h). \tag{3.3}$$

This scaling for g' is compared with the present data in figure 4(*b*), which shows the values of g' from figure 4(*a*) plotted against the independent quantity $B_0^{2/3}W/h^{4/3}$. The level of collapse in this figure is better than the scaling presented in figure 4(*a*), and applicability of both scalings is discussed below. Setting F_3 equal to a constant

in (3.3) gives

$$g' = (3.08 \pm 0.43)\frac{B_0^{2/3} W}{h^{4/3}} \tag{3.4}$$

where the constant F_3 has been evaluated using a least-squares fit, shown as a solid line in figure 4(*b*).

Even though the scatter of g' between the measurements and the least-squared fit to the Maxworthy (1997) model is substantially smaller than the fit to the Phillip's (1966) model the latter still provides a reasonable explanation for the present data. The most probable reason for this is that the flow below the sources was actually a combination of the two. Maxworthy's model assumes, based on experiments, that two active layers would be formed, connected by an overturning region at the closed end. Grimm & Maxworthy (1999) found that this region occupied about 1–2 channel heights i.e. only about 5–10 % of the length of their long channel. Flow in this actively overturning region was exactly of the type described by the model of Phillips (1966). Thus one can think of the total flow, in the present case, as being a combination of a two-layer flow, as in Grimm & Maxworthy (1999), and an actively overturning flow, as in Phillips (1966). The extent to which one or the other dominates depends on the exact geometry being considered. In the present case it seemed that the geometry was such that both were important and this led to the ambiguity in deciding between them. This point of view is supported by the experiments of Finnegan & Ivey (1999), in a convectively driven exchange flow in a short channel, in which no two-layer flow was formed, the whole flow was in the actively overturning mode and was best described by the Phillips (1966) model.

3.2. *Convection in a rotating fluid*

3.2.1. *Experiments with source widths $W = 31$ and 15.5 cm*

As with the non-rotating case, shortly after the supply of dense fluid to the buoyancy source was switched on, a thin dense layer (Ekman layer) began to flow down the slope. However, because of the Coriolis force the direction of the flow was diverted to the left, when looking down the slope, as observed, for example, in similar experiments by Lane-Serff & Baines (1998, hereafter referred to as LB). For most of the rotating cases in the present experiments, the viscous downslope flow eventually became unstable and formed a series of breaking waves with crests that lay approximately perpendicular to the direction of the downslope flow. These waves are similar to the waves that were observed by LB in both rotating and non-rotating experiments and had the appearance of internal roll waves. Later, a boundary current could be observed which ran downslope along the left wall. In some experiments vortices in the dense layer emerged from directly beneath the bouyancy source.

The values of g' measured on the slope and in the boundary current are considered below. The scaling for g' by Maxworthy (1997) (shown in figure 4*b*), will be applied to the data, as it provided a better fit to the data for the non-rotating experiments. The non-dimensional values of g', $G' = g'h^{4/3}/B_0^{2/3}W$, are plotted in figure 5 with respect to the parameter $P = (B_0/f^3h^2)^{1/2}W/h$ to introduce the effects of rotation. This parameter combines the effect of rotation through the natural Rossby number $Ro^* = (B_0/f^3h^2)^{1/2}$, as found in experiments of Maxworthy & Narimousa (1994) and numerics of Jones & Marshall (1993) and Cui & Street (2001). The addition of the scaling W/h was necessary to bring the data into better agreement, as was found also in Maxworthy (2002), after using Ro^* alone resulted in considerable data scatter. The

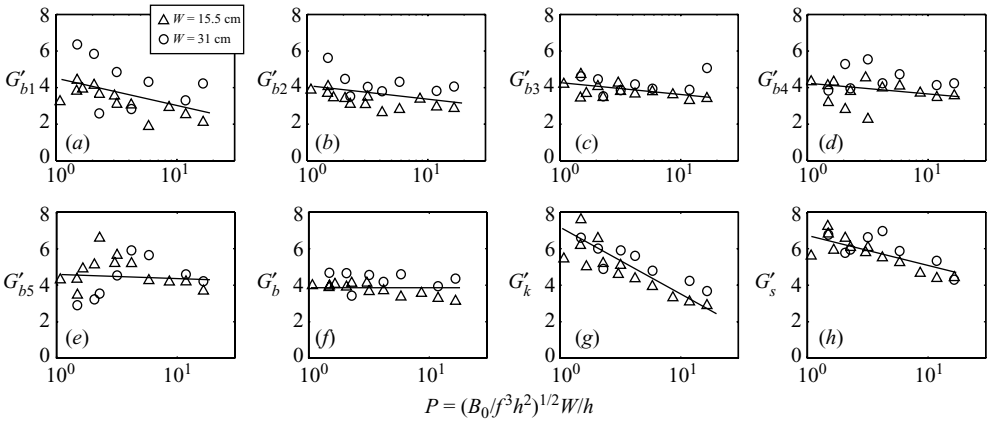

FIGURE 5. The non-dimensional values of g', $G' = g'h/(B_0W)^{2/3}$, are plotted against the independent quantity, $P = Ro^*W/h = (B_0/f^3h^2)^{1/2}W/h$. (*a–e*) $G'_b = 1$ to 5 calculated from measurement at the bottom of the five downslope reservoirs (marked as 1–5 in figure 2), (*f*) $G'_b = 3.86 \pm 0.54$ for the mean of dense flow on the slope, (*g*, *h*) $G'_K = 3$ to 7 for the Kelvin current (marked as 6 in figure 2), and G'_s for bottom flow measured on the middle-hand of the shelf close to the left-hand wall (marked as 7 in figure 2).

scaling appears to collapse the data for the range of B_0, W, h and f of the present experiments.

$G'_{b_{1-5}}$ in figure 5(*a–e*) is calculated from measurements at the bottom of each of the five reservoirs downslope, marked as 1–5 in figure 2. Figure 5(*f*) shows a straight average of these measurements, i.e. $G'_b = (G'_{b_1} + G'_{b_2} + G'_{b_3} + G'_{b_4} + G'_{b_5})/5$. G'_K in figure 5(*g*) shows the buoyancy measured in the Kelvin current, marked as 6 in figure 2, and G'_s in figure 5(*h*) shows the buoyancy of the bottom flow on the middle of the shelf and close to the left wall (marked as 7 in figure 2). Here subscripts b, K and s stand for bottom layer, Kelvin current and flow on shelf respectively.

Figure 6 presents schematic diagrams of the mean flows observed, using dye, beneath the buoyancy source in the present experiments. Each diagram shows a plan view of the entire buoyancy source with the slope located above the source region. The solid arrows show the mean flow in the upper layer of the exchange flow, which descended to form the lower layer in a region close to the backwall of the tank, located on the opposite side of the buoyancy source from the slope. The dashed arrows show the mean flow in the dense lower layer. For the non-rotating experiments (figure 6*a*), the mean exchange flow was approximately two-dimensional, with the fresh fluid entering at one location in the upper layer, then leaving directly below as dense fluid in the lower layer. The dense source was approximately uniform in the horizontal direction. In the rotating case (figure 6*b*), however, the exchange flow was changed by the Coriolis force. It was observed that the fluid in the upper layer tended to be diverted to the right, looking downslope, as it flowed under the source towards the backwall of the tank. In the lower layer a large portion of the dense fluid flowed along the whole length of the backwall of the buoyancy source, eventually reaching the left wall of the tank and forming a boundary Kelvin current, marked as s_4 at the shelf–slope edge in figure 6(b). Near the right sidewall (see figure 6(*b*) there was much less motion in the across-slope direction (because of the presence of the wall) and the exchange resembled that in the non-rotating tank. This location also corresponded to one of the three regions (s_1, s_2 and s_3 in figure 6*b*) where domes of dense fluid

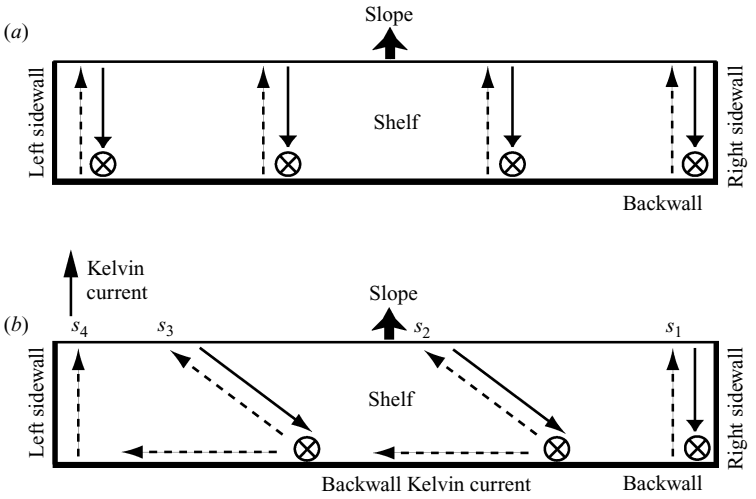

FIGURE 6. Schematic diagram showing the exchange flows beneath the buoyancy source in (*a*) the non-rotating experiments, and (*b*) the rotating experiments. The solid arrows and dashed arrows represent the fluid flows in the upper fresh and lower dense layers, respectively.

appeared from beneath the source. At large rotation rates, domes or eddies of dense fluid were generated periodically at s_1 and then propagated towards the left wall. The two regions, s_2 around the middle of the shelf and s_3 close to the left wall, were also sources of domes of dense fluid. It is noted that vortices, if created, appeared almost stationary at s_2 and s_3. With the wider dense source, e.g. when its width equalled that of the shelf, i.e. $W = 31$ cm, the mean dense flow was found to be weak at s_2 and eddies never formed there. At very large rotation rates, vortices generated at s_3 could even propagate towards the right-hand side, i.e. against the Coriolis force. Details of these flow regimes can be found in § 3.3.

3.2.2. *Experiments with a narrow, $W = 2$ cm wide, source*

To investigate changes in the flow with the width of the buoyancy source, rotating experiments were performed with a very narrow shelf and source ($W = 2$ cm rather than $W = 31$ cm or 15.5 cm), i.e. one not much larger than the width of the Kelvin current along the backwall. In these experiments the observed behaviour of the mean flow under the buoyancy source was qualitatively similar to the experiments with $W = 31$ cm or 15.5 cm, and suggests that the exchange flow depicted in figure 6(*b*) is robust to changes in the source's aspect ratio.

Even though the dense outflow became non-uniform along the shelf in the rotating experiments, turbulent convection underneath the dense source seemed not to be affected, except at the left wall where a strong boundary current was generated. It is noted that the mean reduced gravity of the bottom flow measured at reservoirs 1 to 5 in the rotating experiments was $G'_b = 3.86$ (figure 5*f*), this being different to the non-rotating experiments $G'_b = 3.08$ (equation (3.4)). Figures 5(*g*) and 5(*h*) show a large increase in the density for the Kelvin current and the dense flow close to the left side as P decreased. This implies an increased effect due to the boundary (both back and sidewalls) when the ratio L/W or the rotation rate became large (i.e. smaller P). The effect of the proximity of the right wall also caused a notable increase of the density (measured at the downslope reservoir 1) as P decreased (shown in figure 5*a*).

3.3. *Flow morphology*

This section concerns the morphology of the structures in the bottom layer as they formed on the shelf and flowed down the slope. The flow conditions can be divided into five regimes depending on the value of $P = (B_0/f^3h^2)^{1/2}W/h$, the modified natural Rossby number.

3.3.1. *Non-rotating experiments, i.e. $P = \infty$: laminar Ekman layer*

In this case, the downslope bottom layer flowed perpendicular to contours of constant depth. It stayed laminar and no waves or eddies were visible. The layer was observed to be sensitive to external noise and would produce waves if slightly disturbed, indicating the existence of a convective type of instability.

3.3.2. *$14 < P < 45$: roll waves formed on the Ekman layer*

With the tank rotating, the bottom layer still continuously flowed down but at an angle to contours of the constant depth under the effect of the Coriolis force, e.g. 70° at the modified, natural Rossby number $P = 18$. For values of $P < 45$, roll waves were produced in the dense bottom layer.

In all of the rotating experiments a boundary Kelvin current (see Griffiths & Hopfinger 1983) was formed on the left wall of the tank, when looking downslope, which ran down the slope (marked as s_4 in figure 6*b*). The majority of the dense fluid in the boundary current appeared to come directly from beneath the buoyancy source (viewed by adding dye to selected regions of the buoyancy source). The density of the boundary current was larger than the dense fluid on the slope.

3.3.3. *$5.5 < P < 14$: periodic release, or 'surges', of dense fluid*

Here no distinct vortices were observed; however a periodic release of dense fluid, or 'surges', appeared from underneath the dense source and flowed downslope. This represents a transition regime, as the dense flow changed from emerging along the whole shelf (at $P > 14$) to conditions where it started to collect in localized regions (at $P < 5.5$). The period of release was equal to one rotation period, T. As the tank rotated faster, the angle (to contours of constant depth) of the bottom flow decreased, e.g. 65° at $P = 66$. Roll waves formed in the bottom layer on the slope.

3.3.4. *$P < 5.5$: eddies propagating along the shelf or slope*

In all of the experiments where vortices were produced, they were observed to emerge from the buoyancy source in three localized regions, s_1, s_2 and s_3 in figure 6(*b*). The localized sources of vortices at s_1 and s_3 are believed to be a result of the close proximity of the right- and left-hand walls. This is different from experiments which have used an axisymmetric topography such as a truncated cone (Jacobs & Ivey 1998; LB) or a flat, circular, horizontal bottom (Maxworthy & Narimousa 1994; Narimousa 1997), where vortices have been reported to be produced randomly around the full circumference of the buoyancy sources.

Observations by LB surggest that the flux of dense fluid in a layer moving downslope is modulated by the presence of vortices/eddies. This was also true in the present experiments where the release of a surge of dense fluid accompanied the production of an eddy. An example of such a release may seen in figure 7 with eddies marked as e_1, e_2 and e_3. After the initial release, the velocity field of the eddies appeared to inhibit the supply of fluid to the downslope flow. Once created, the eddies (e_1), moved along the slope (figure 7*a*) under the effect of the Coriolis force, i.e. from right to left when looking downslope. As the vortices moved across the slope, they approximately

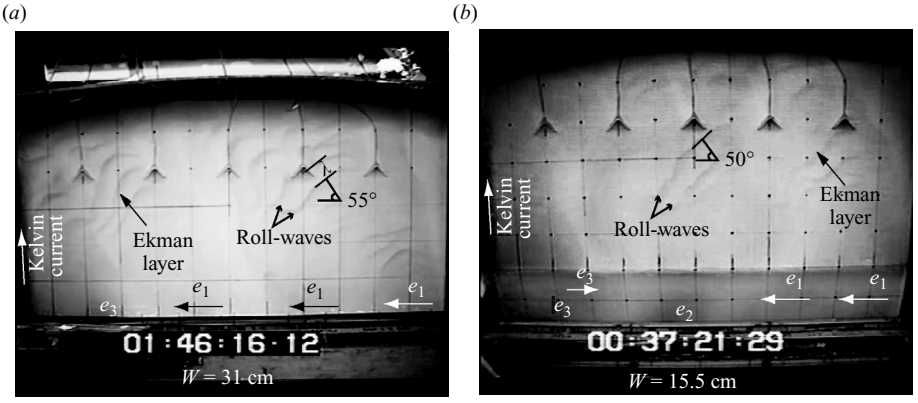

FIGURE 7. Bottom water formation for small $P = (B_0/f^3h^2)^{1/2}W/h$ when eddies were generated with a period of $2T$. (*a*) At $P = 4.9$ and $W = 31$ cm, meso-scale eddies were either stationary, e.g. e_3, or propagated along the slope, e.g. e_1 (the arrows point in the propagation direction). (*b*) At smaller P, e.g. $P = 2.2$ with smaller $W = 15.5$ cm, a stationary eddy e_2 appeared around the centre of the shelf. At the same time eddy e_3 propagated to the right, i.e. against the Coriolis force.

followed lines of constant depth. The eddies (e_1) were produced at s_1 with a period $2T$, twice that of the rotation period.

For smaller values of the modified natural Rossby number, P, the progress of eddies across the slope was not regular, with eddies wandering back and forth in the across-slope direction. With $P < 2.8$, especially with the relatively narrow dense source, $W = 15.5$ cm, a visible displacement in the opposite direction to the Coriolis force was observed in the eddies close to the left-hand wall, e.g. e_3 in figure 7(*b*) (e_3 moved from left to right when looking downslope). Similar counter-intuitive displacements have been reported by Mory, Stern & Griffiths (1987) and LB. One probable reason for the present observations was the increased effect of the concave water surface at large rotation rates. This concave effect caused a slightly higher water depth at the left- and right-hand walls than at the tank centre.

Dense fluid was observed to be released from the eddies and then propagated downslope. The angle to contours of constant depth reduced as P decreased, e.g. 55° at $P = 24$ (figure 7*a*), and 50° at $P = 2.2$ (figure 7*b*).

3.4. *Wave and eddy production*

3.4.1. *Criteria for eddy formation*

LB presented a model and criteria for the generation of vortices in rotating flows on a slope, also see Condie (1995) and Baines & Condie (1998). For a viscous flow moving along and down a slope, i.e. an Ekman type layer, LB among others have suggested appropriate scalings for its alongslope velocity, $c_v = \alpha g'/f$, when gravity balances the Coriolis force, and the Ekman layer thickness $d_v = (2\nu/f)^{1/2}$, where α is the slope angle from the horizontal, 15° in the present experiment, and ν is the kinematic viscosity of water. Based on their model, LB stated that vortices can only form if the loss of dense fluid due to viscous downslope drainage into the viscous layer described above does not dominate the flow. For an inviscid current moving along a slope (see Griffiths & Hopfinger 1983), LB introduced an alongslope length

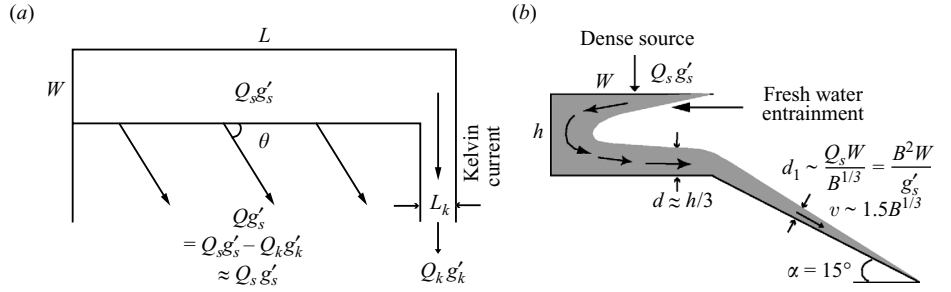

FIGURE 8. Dense flow geometry. (*a*) Estimation of the buoyancy flux in the downslope current. As shown in the text, it is assumed that $Q_k g'_k \ll Q_s g'_s$ and this was found to be so *a posteriori*. (*b*) Volume fluxes of dense flow from under the source and in the downslope Ekman layer. Here, d_1 is the thickness of the Ekman layer based on buoyancy flux estimation in (*a*), and v is the downslope velocity of the Ekman layer as found at the end of this subsection § 3.4.1.

scale Y over which dense fluid drained from the current,

$$Y = \frac{Q}{c_v d_v} = \frac{Q f^{3/2}}{g' \alpha (2\nu)^{1/2}}, \tag{3.5}$$

where Q is the volume flux of fluid into the inviscid current.

The ratio of this alongslope drainage distance to the width of the current was taken to be a measure of the relative importance of viscous drainage from the current, and is given by $F = Y/L_{Ro}$ where the width of the current was taken to scale with the Rossby radius of deformation $L_{Ro} = (g'd)^{1/2}/f$ (following the results of Griffiths & Hopfinger 1983), and d is the depth of dense current upstream. For vortices to form, this ratio must be sufficiently large, so that the distance the current travels, Y, before the volume flux of dense fluid, Q, has drained downslope is significant compared with L_{Ro}.

Unlike the experiments of LB, in which Q and d were set, in our case the volume flux of dense fluid from the buoyancy sources and the height of the dense current on the shelf were dependent quantities. Before estimating the downslope volume flux Q, it was necessary to verify that the amount contributing to the Kelvin current along the sidewall, Q_k, was small compared with Q (see figure 8*a*). The triangular cross-sectional area of the Kelvin current was approximately $L_k^2/2$, where L_k is the Rossby radius of the fluid in that current, given by $B^{1/3}/f$, since *a posteriori* we show that the downslope velocity is of order $B^{1/3}$. Thus the buoyancy flow rate through the Kelvin current is $L_k^2 B^{1/3}/2$. Then the ratio of the flux in the Kelvin current to that of the dense fluid source becomes

$$\frac{L_k^2 B^{1/3} g'_k}{2 Q_s g'_s} = \frac{B g'_k}{2 f^2 Q_s g'_s} = \frac{Q_s g'_s g'_k}{2 L f^2 Q_s g'_s} = \frac{g'_k}{2 L f^2}, \tag{3.6}$$

where Q_s and g'_s are the volume flux and the reduced gravity for the dense fluid source, and Q and g'_b are corresponding values for the downslope bottom layer. This ratio is typically less than 0.15 and to a good degree of approximation $Q_s g'_s \approx Q g'_b$.

The height of the upstream dense flow, i.e d in LB, was observed to be around $h/3$ on the shelf in the present experiments, where h is the height of the buoyancy source above the shelf (figure 8*b*). This thickness, $d = h/3$, is consistent with the edge of the shelf being a hydraulic control. For most cases, the thickness of upstream dense flow was much larger than that of the downslope Ekman layer, i.e. $d \gg d_v$. Instead

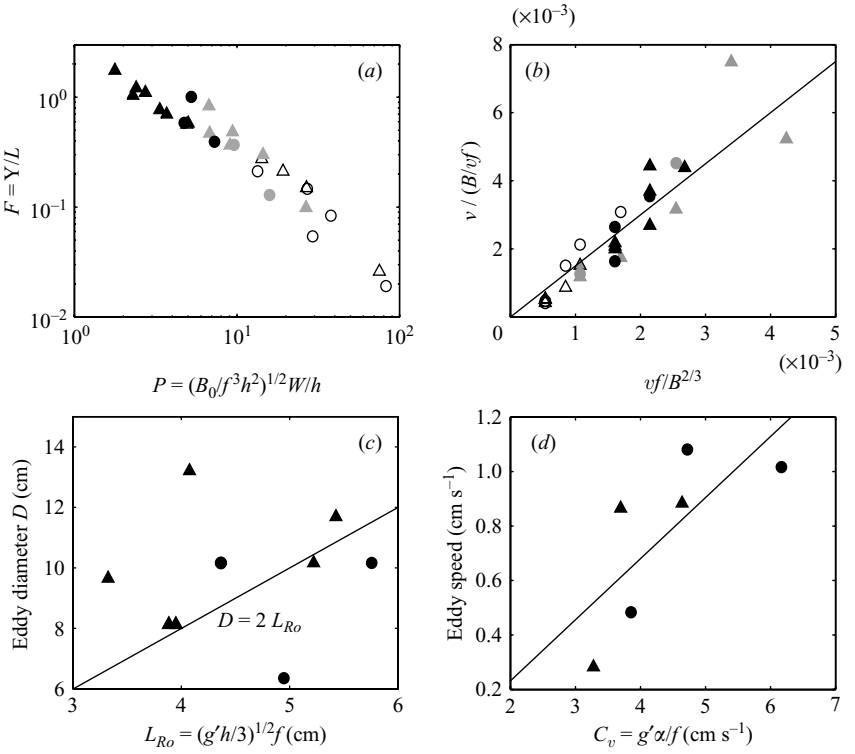

FIGURE 9. Vortex and Ekman layer production. (*a*) Flow regimes at different Y/L and $P = (B_0/f^3h^2)^{1/2}W/h$. (*b*) The downslope velocity of the Ekman layer, v, scales with $(B_0W)^{1/3}$, i.e. $vvf/B_0W = 1.5vf/(B_0W)^{2/3}$. (*c*) The measured eddy size (diameter D) versus the Rossby deformation radius, $2L_{Ro} = 2(g'h/3)^{1/2}/f$. (*d*) The eddy velocity alongslope as a function of the 'Nof speed', $c_v = g'\alpha/f$, Nof (1983). Triangles: $W = 15.5$ cm, circles: $W = 31$ cm; solid symbols, eddies; grey symbols, periodic release; open symbols, continuous release.

of the Rossby deformation radius, L_{Ro}, used by LB to scale the unknown alongslope length of the dense current upstream, here, the length of the dense source is directly related to the length of the dense current, $L = 120.5$ cm (also see Condie 1995). Then $F = Y/L = Q/Ld_vc_v$ a measure of the relative importance of viscous drainage from the dense source, was used to specify the flow regime.

Figure 9(*a*) is a regime diagram using the parameter space prescribed by $F = Y/L$ and $P = Ro^*W/h = (B_0/f^3h^2)^{1/2}W/h$ (the modified natural Rossby number). Each of the rotating experiments is represented by a different symbol depending on the flow observed. The solid symbols show experiments in which definite evidence of vortices/eddies was observed, the grey symbols show those in which there were periodic releases of dense fluid, and the open ones show cases where continuous release of dense fluid was generated. Similar to observation by Condie (1995), LB and Baines & Condie (1998), eddies were generated at relatively large F, despite differences in the source condition. The criterion reported in LB, $F \geqslant O(1)$, is larger than the value observed in the present experiments, $F \geqslant 0.3$. This is reasonable considering the fact that our calculation is based on a larger alongslope length scale, $L > L_{Ro}$.

The downslope speed of roll waves was used as an approximate estimate of the downslope velocity v of the dense bottom flow by assuming very approximately that the waves were being convected with the mean velocity of the current, but see below.

These measurements are plotted in figure 9(*b*). A scaling for the downslope velocity of an Ekman layer proposed by Nagata *et al.* (1993) and Baines & Condie (1998), $v \sim \alpha g'/f$, was investigated and found to be inappropriate in the present case. A more appropriate scaling for v, obtained by dimensional analysis, is proposed below and will be shown to model the present data well.

Dimensional analysis using the independent variables of the downslope flow, B, f and ν gives

$$v = \frac{B}{\nu f} \cdot \text{func}\left(\frac{\nu f}{B^{2/3}}\right) \tag{3.7}$$

where $B/\nu f$ is one possible velocity scale and $\nu f/B^{2/3}$ is a dimensionless parameter. Since α is a constant here, it is ignored. By assuming a power-law relationship for the function func, velocity scales can be constructed of the form

$$\frac{B}{\nu f}\left(\frac{\nu f}{B^{2/3}}\right)^{\beta}, \tag{3.8}$$

where β is an arbitrary integer.

Figure 9(*b*) suggests that a linear relationship exists between $B/\nu f$ and $\nu f/B^{2/3}$, i.e. $\beta = 1$, so that

$$\frac{v}{B/\nu f} = 1.5\frac{\nu f}{B^{2/3}} \Longrightarrow \frac{v}{B^{1/3}} = 1.5. \tag{3.9}$$

The coefficient 1.5 is obtained from the linear least-square fit to the experiment data. Note that in figure 3, the scaling for the time before the system reached its quasi-steady state also implies that the downslope velocity scales as $(B_0 W)^{1/3} = B^{1/3}$. It is this result that was used to evaluate (3.6). Here, ignoring the slope angle effect α in obtaining (3.9) means that the result is only valid for the particular value 15° tested in our experiments.

3.4.2. *Eddy dynamics*

The eddies produced in the rotating experiments took the form of isolated 'domes' of dense fluid which moved across the slope, leaking dense fluid into the Ekman layer as they did so. The ambient fluid directly above the domes was observed to rotate cyclonically, using particles and dye on the water surface. The vorticity of the domes could not be determined. However, it was expected to be anticyclonic, in accordance with related experiments by Maxworthy & Narimousa (1994), Narimousa (1997), LB and Jacobs & Ivey (1998).

Eddy size and propagation speed were measured for those generated at the right-hand side of the tank that then migrated to the other side of the tank, along the slope, i.e. from s_1 to s_4 in figure 6. Eddies formed at other locations had the similar size but were either stationary or moving irregularly. Figure 9(*c*) shows the measured eddy diameter D plotted against the Rossby deformation radius L_{Ro}, together with the line $D = 2L_{Ro}$. As can be seen from the figure, the data are very scattered. However, an eddy diameter of around twice L_{Ro} appears to best represent the data.

Figure 9(*d*) shows the eddy propagation speed along the slope in those experiments where the migration was regular enough to make measurements. As can be seen from the figure, the eddy propagation speed alongslope scales well with a relationship proposed by LB to model an isolated volume of dense fluid that moved along a slope under the balance of gravity and the Coriolis force, via the 'Nof speed', $c_v = \alpha g'/f$ (Nof 1983).

To model the rate at which eddies are generated, LB assumed that if domes of dense fluid can be approximated by cylinders of radius L_{Ro} and height d, then the time for each cylinder to fill may be expected to scale as

$$\frac{\pi L_{Ro}^2 d}{Q} = \frac{2\pi}{f} = T/2, \tag{3.10}$$

where $\pi L_{Ro}^2 d$ is the volume of each cylinder and $Q \sim dL_{Ro}u/2$, $u \sim (g'd)^{1/2}$ is the velocity of the current given by a standard gravity current model (see Griffiths & Hopfinger 1983).

The mean time interval T_{int} between the formation of successive vortices, i.e. those represented by solid symbols in figure 9, was found to be around two rotation periods $2T$. Following (3.10), this corresponds to $T_{int} = 4 \times (2\pi/f)$. Although LB modelled their vortex generation rate differently from the present study, at large f, which is in keeping with the range of f covered here, their modelling gives $T_{int} = 4.8 \times (2\pi/f)$. The value of the constant in LB's relationship is close to the present value, which supports the use of the above modelling. The mean time interval between successive releases of dense fluid when vortices were not generated, i.e. the grey symbols for dense surges in figure 9, was measured to be around one revolution period, T.

4. Convection into and down a submarine canyon

Topographic variations, e.g. submarine canyons, can contribute significantly to the local downslope flow by channelling the heavy basal fluid (Baines & Condie 1998). The effect of a canyon has been introduced into the present investigations over a wide range of flow conditions. The canyon was located at around one third of the length of the shelf–slope and stretched from the middle of the shelf to the bottom of the slope (see figure 2). It was thought that positioning the canyon $L/3$ away from the left wall (when looking down slope), rather than the centre, would mean that the flow into the canyon would not be influenced by the eddy production at the right-hand wall.

Again, the density of the downslope bottom fluid (using reservoirs $1-5$ in figure 2), the Kelvin current (marked as 6) and the bottom fluid channelled into the canyon (marked as 8) was measured.

4.1. *Convection in a non-rotating fluid*

The reduced gravity of the bottom fluid on the slope and in the canyon are plotted in figure 10 following the scalings proposed by Phillips (1966) (figure 10*a*) and by Maxworthy (1997) (figure 10*b*). As with figure 4, there is a slightly better collapse of data using Maxworthy's (1996, 1997) scaling.

By comparing figure 10 and figure 4, it can be seen that the reduced gravity of the downslope flow (outside the canyon) is not much changed by the presence of the canyon. The slight difference is believed to be due to a small systematic error caused by the difference in the alignment of the shelf–slope structure before and after removing the tank insert when the canyon was cut.

For the largest values of $(B_0 W)^{2/3}/h$ and $B_0^{2/3} W/h^{4/3}$, the density in the canyon becomes significantly larger than the value measured in reservoirs down the slope. Under this condition, the canyon (extending partly across the shelf) could channel away part of the dense fluid directly beneath the source trays before it was mixed/diluted further with fresh water. The errors between the density of the five reservoirs is larger than in figure 4, which is likely to be due to the regional effect of

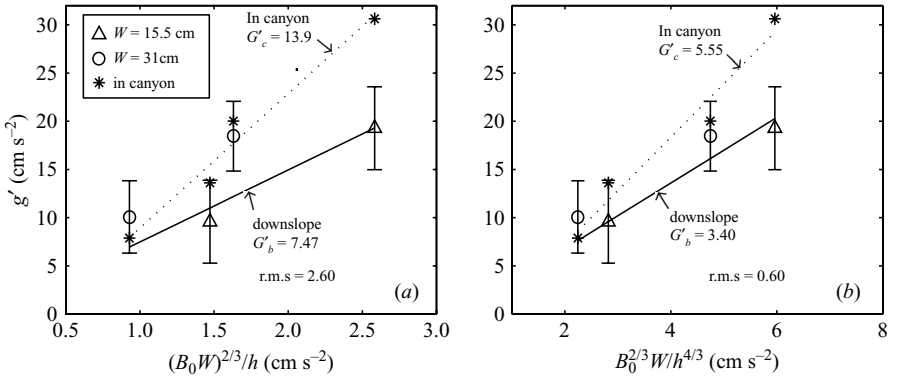

FIGURE 10. The reduced gravity, g', of the dense downslope flow with a canyon in a non-rotating fluid is plotted following two different scalings, (*a*) $g'_b = (7.47 \pm 2.60)(B_0W)^{2/3}/h$ proposed by Phillips (1966) and (*b*) $g'_b = (3.40 \pm 0.60)B_0^{2/3}W/h^{4/3}$ proposed by Maxworthy (1996, 1997). The mean of the data collected at the five reservoirs, 1–5, is plotted with the error bars reflecting the difference between the maximum and the minimum. Data collected in the canyon are marked by a dotted line and the asterisk symbol. A linear least-square fit to data collected in the canyon gives $G'_c = 13.9$ following the Phillips model, and $G'_c = 5.55$ when fitted to the Maxworthy model. Values are larger than that for the down slope flow, i.e. $G'_c > G'_b$.

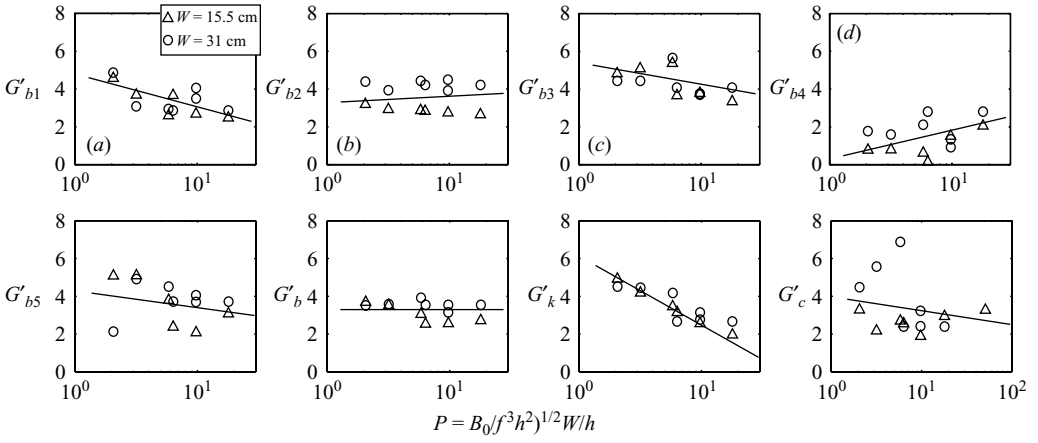

FIGURE 11. The non-dimensional values of g', $G' = g'h^{4/3}/B_0^{2/3}W$, are plotted for flow with a canyon against the independent quantity (the modified, natural Rossby number), $P = (B_0/f^3h^2)^{1/2}W/h$. (*a–e*) $G'_{b_{1-5}}$ is calculated from measurement at the bottom of these five reservoirs downslope (marked as 1–5 in figure 2), again $G'_b = 1$ to 5 except for the one just downstream of the canyon, i.e. $G'_{b_4} = 0$ to 2 for reservoir 4; (*f*) $G'_b = 3.30 \pm 0.44$ for a straight average of dense flow on the slope collected in reservoirs 1–5. (*g*) $G'_K = 1$ to 5 for the Kelvin current downslope (marked as 6 in figure 2); and (*h*) $G'_c = 6$ to 11 for bottom flow in the canyon (marked as 8 in figure 2).

the canyon and, possibly, the introduction of non-uniformity during the shelf/slope reconstruction.

4.2. *Convection in rotating fluid*

The buoyancy of the bottom flow channelled in the canyon (figure 11*h*), was found to be significantly larger than that of the downslope flow and Kelvin current (figure 11*a–e*, *g*). The density of the downslope flow to the left of the canyon

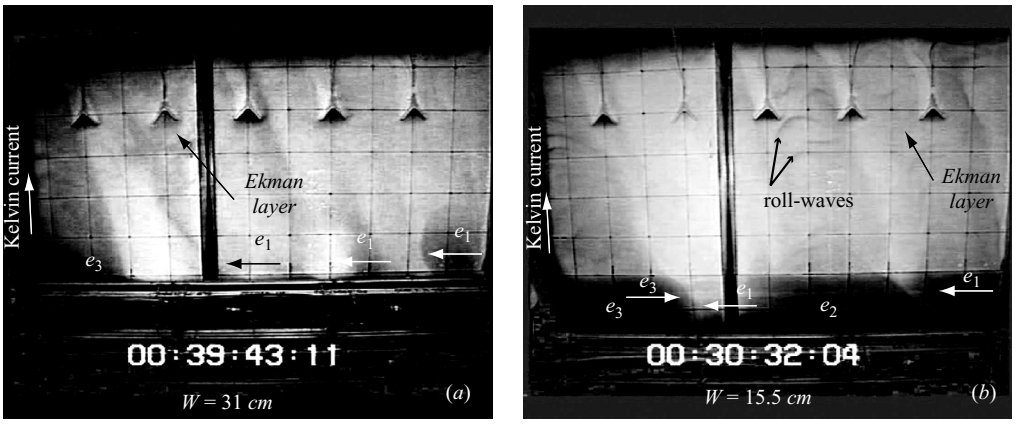

FIGURE 12. Bottom water formation for small $P = (B_0/f^3h^2)^{1/2}W/h$, with a canyon cut from the middle of the shelf to the bottom of the slope: (*a*) at $P = 4.8$ and $W = 31$ cm (a similar parameter space is covered in figure 7*a* before the canyon was cut) the eddy e_1 and the downslope Ekman layer were able to travel across the the canyon; (*b*) at $P = 3.5$ with $W = 15.5$ cm (a similar parameter space is covered in figure 7*b* without the canyon) again the eddy e_1 was able to cross the canyon on the shelf.

(when looking downslope), shown in figure 11(*d*), can clearly be seen to be reduced by the presence of the canyon, particularly at small values of P. In this case, the canyon clearly interfered with the downslope flow and captured most of the dense fluid passing through, leaving the bottom fluid downstream with a reduced density. A slight density reduction existed in the straight average of downslope dense flow, $G'_b = (G'_{b_1} + G'_{b_2} + G'_{b_3} + G'_{b_4} + G'_{b_5})/5$ ($G'_b = 3.30$ in figure 11*f*), compared with the value before the canyon was cut ($G'_b = 3.86$ in figure 5*f*). The value of G'_K in the Kelvin current (figure 11*g*) was also somewhat reduced by the presence of the canyon compared to before the canyon was cut (see figure 5*g*). If the flow above the shelf is considered (see figure 6*b*), then it may be expected that a canyon (extending partly across the shelf) will channel away part of the dense fluid that flows along the backwall before forming a downslope Kelvin current. Thus, the effect of canyon here also reduced the supply of the densest fluid to the downslope Kelvin current, as shown in figure 11(*g*).

4.3. *Flow morphology*

The characteristics of bottom water flow regimes (namely, continuous release of dense flow with roll waves appearing in the downslope Ekman layer, periodic surges of dense flow, and of eddies) were observed to be similar to those without the canyon (figure 9*a*), even though the existence of the canyon weakened the Ekman layer and the eddies that propagated towards the canyon.

For all the experiments, the canyon entrained dense fluid from the bottom layer and channelled it downslope. This withdrawal started from the middle of the shelf at the canyon head and the current increased with further injection of fluid from the Ekman layer as the channelled fluid descended towards the bottom of the slope. An experiment with a relatively small value of the modified natural Rossby number $P = (B_0/f^3h^2)^{1/2}W/h$ was chosen for figure 12(*a*). It can be seen that both the eddy e_1 and the downslope Ekman layer with superimposed waves travelled across the canyon. In figure 12(*b*) under even smaller P, part of the dense fluid from the eddy e_3 moved towards the canyon against the Coriolis force.

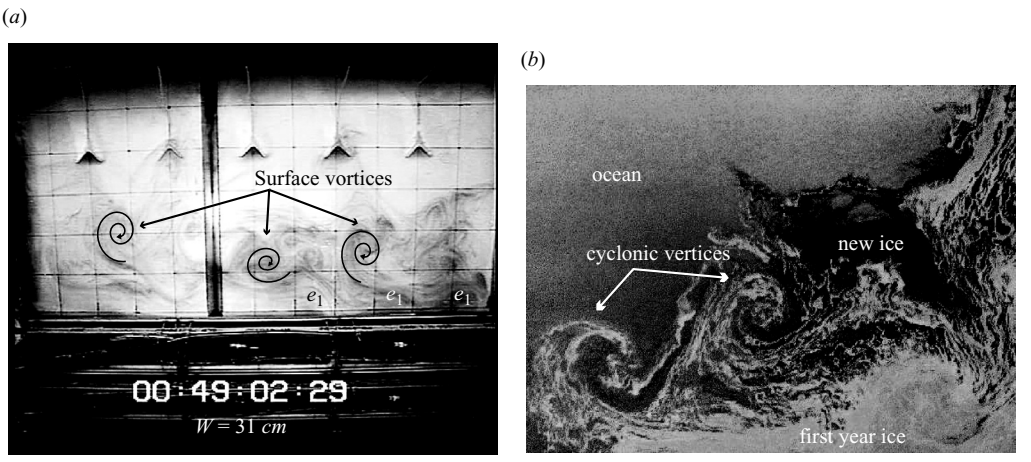

FIGURE 13. Surface cyclonic vortices. (*a*) Under the same condition as in figure 12(*a*) with $P = 4.8$, $W = 31$ cm, surface cyclonic vortices illustrated by dye dropped onto the water surface. (*b*) A radar image (240 km by 360 km) taken by the Shuttle Imaging Radar-C (image provided by Jet Propulsion Laboratory) shows two large ocean eddies next to sea ice in the Weddell Sea, Antarctica, on October 5, 1994.

Surface cyclonic vortices made visible by dye dropped onto the water surface are shown in figure 13(*a*). They appear to be similar to cyclonic ocean eddies observed in the Weddell Sea (figure 13*b* from Jet Propulsion Laboratory Image Gallery†). The latter eddies were made visible as freely-floating sea ice was swept around in their rotating currents.

5. Conclusions and discussion

The experiments reported here have investigated convection and bottom water formation in a rotating fluid with a sloping bottom. The aim of the experiments was to model the exchange flows occurring over a continental shelf in polar regions (e.g. the Weddell Sea, Ross Sea or Arctic coast) and to study their behaviour on the continental slope.

In the experiments a negative buoyancy flux was applied to the free surface of the fluid directly above a horizontal shelf. The dense convection products that formed over the shelf flowed under the effects of gravity and rotation over a plane slope, fixed at 15° to the horizontal. For experiments performed in a non-rotating fluid, two existing models (proposed by Phillips 1966 and Maxworthy 1996, 1997, respectively) were tested using the experimental data. For the parameter ranges considered, both models provided a good collapse of the data, possibly suggesting that the present flow type lay somewhere between the two models proposed.

Experiments were also performed with the tank rotating. The three-dimensional turbulence driven by convection over the shelf was not notably affected by rotation (consistent with the findings of Maxworthy & Narimousa 1994, Narimousa 1997 and Jacobs & Ivey 1998). The density of the dense layer on the slope also was not strongly affected by rotation, as can be seen by comparing values of G'_b, 3.08 ± 0.43 in figure 4(*b*) and 4 ± 0.5 in figure 5(*f*). However, the mean exchange flow was changed.

† http://southport.jpl.nasa.gov/polar/sarimages.html.

This is shown schematically in figure 6. A feature of some of the rotating experiments was the generation of vortices. These vortices might take the form of anticyclonic domes of dense fluid (with cyclonic vorticity in the fresh ambient directly above them). We suggest this direction based on the assumption of vorticity conservation though which surface cyclonic eddies could have formed anticyclonic eddies in the bottom dense layer. The eddies in the bottom layer either were stationary or moved across the slope approximately following lines of constant depth. Vortices were not generated in all of the rotating experiments, and criteria based on parameters, the modified natural Rossby number $P = (B_0/f^3h^2)^{1/2}W/h$ and the relative importance of viscous drainage from the dense source $F = Y/L = Qf^{3/2}/\alpha g'(2\nu)^{1/2}W$, were found to be applicable to the present experiments. Under certain conditions, the frequency at which the vortices were produced compared favourably with similar experiments by LB, and the eddies, when produced, had a size comparable to the Rossby deformation radius $L_{Ro} = (g'h)^{1/2}/f$. When eddies propagated along the slope (starting from position s_1 in figure 6*b*), their speed was shown (in figure 9*d*) to be well represented by $c_v = \alpha g'/f$ (Nof 1983), in accordance with a model used in LB.

Unlike many experiments which have used an axisymmetric topography (see Maxworthy & Narimousa 1994; Narimousa 1997; LB; Jacobs & Ivey 1998), the presence of the sidewalls of the tank was found to have a profound effect on the generated vortices, which emerged from the buoyancy source only at localized regions. In particular, the region close to the right-hand wall, when looking downslope, was the location where most of the dense fluid emerged from under the buoyancy source, often in the form of a periodic release of fluid. A portion of the dense fluid flowed along the backwall of the tank. It then turned and formed a boundary current which flowed down the slope against the left-hand wall in the form of a Kelvin current in which the Coriolis force balanced transverse pressure gradients (see figures 2 and 6*b*). The flux through the Kelvin current has been shown to be small compared with downslope flux.

Bottom water formation has been studied extensively here over a wide range of B_0, f, h and W. For different conditions, the bottom layer had different characteristics: e.g. quasi-steady laminar flow at $P = \infty$; continuous release of dense flow with roll waves forming in a downslope Ekman layer as $14 < P < 45$; periodic release of dense flow at a frequency of one revolution, $1/T$, when $5.5 < P < 14$; and stationary and propagating eddies for $P < 5.5$, which were generated with a period of $2T$. All eddies observed in our case leaked dense fluid into the Ekman layer. For all the rotating experiments, roll waves were observed to form and propagate downslope with the Ekman layer. The wave speed was used to crudely estimate the total downslope velocity of the Ekman layer and it was found to be of the form $v \sim (B_0 W)^{1/3}$. The Ekman layer was observed to travel down the slope towards the left-hand wall at an angle to contours of the constant depth. This angle decreases as the value of P decreases, e.g. 70°, 65°, 55°, 50° for $P = 18$, 8.1, 4.9, 2.2 respectively.

Attempts have been made to relate the results of these experiments, e.g. estimates of bottom-water density, to observations in the seas around the Antarctic continent but criticism, from various sources, led to their being abandoned. The main problem lies in the paucity of observational data at the geographical locations where one would expect the heavy bottom water to be formed. For example, in Whitworth *et al.* (1998) the emphasis is on water properties near the shelf break; in particular, they clearly show the approximately 200 m thick dense-layer flowing down the continental shelf in clear agreement with the present experimental observations. However, the actual regions of dense water formation were likely to have been outside their observational

area. In general actual bottom topography and depth variations are far more complex than assumed in the present simple model. Also, estimates of the magnitude of the surface buoyancy flux in the natural situation were not available and so one was left to guess a value based on dubious assumptions. Finally, the widths, total areas and locations of the regions subjected to this flux are highly variable depending, as they do, on the existence of areas of open water, polynas, that are transitory in time and unevenly distributed in space (see e.g. Bromwich *et al.* 1998). Thus, the present model, while it gives a valuable qualitative picture of the natural flow, is, unfortunately, marginally useful as a tool for predicting the details of any existing set of field observations.

An attempt is made to relate our experimental observations of roll-wave formation to theories looking at this matter. One of a few such theories is the Swaters (2003) theory, which considers a thin viscous layer underlying a stratified upper deep layer, with the 'roll waves' that develop on the former forcing internal waves in the latter. As an example consider the waves observed in figure 7(*a*, *b*). Here the wavelength varies from about 2 to 5 cm with wave fronts propagating at angles between 50° and 55° to the lines of constant depth. Their total velocity is of the order of 3 cm s^{-1} and this magnitude is the result of adding the velocity, V, of the unknown underlying mean flow to that of long waves with velocity $(g'h_v)^{1/2}$, with h_v the thickness of the viscous thin layer.

Here we concentrate on the lower layer in the Swaters (2003) theory, since in the present experiments the upper layer was not stratified. The theory contains two independent variables that are known exactly, i.e. f and bottom slope, $\tan\alpha$, and four that are dependent and have to be either measured or estimated, i.e. bottom layer reduced gravity, g', thin layer thickness, h_v, a modified drag coefficient, C_D and dimensionless Coriolis parameter, $\mathscr{F}$. Values of g' come from direct measurements, i.e. equations (3.1) and (3.4), while for h_v, $\mathscr{F}$ and C_D one needs either a model or an interpretation of the theory that is consistent with the observations outlined above. In Swaters (2003) the following quantities are defined: the dimensionless Coriolis parameter $\mathscr{F} = (4\pi/T)h_v/g'^{1/2}/\tan\alpha$, where T is the period of rotation, and modified drag coefficient $C_D = C_d/\tan\alpha$, where C_d is the drag coefficient. In order to proceed, it is necessary to make some simplifying assumptions. First, in the Swaters expression for the mean velocity, V, if the term in $\mathscr{F}$ is set to zero then $V = (g'h_v)^{1/2}/C_D^{1/2}$. This approximation will be justified after the final result is presented. Eliminating the term $(g'h_v)^{1//2}$ from the expressions for V and $\mathscr{F}$ gives

$$\mathscr{F} = 4\pi V C_D^{1/2}/Tg'\tan\alpha.$$

At this point it is necessary to guess a value for V, with T, g' and $\tan\alpha$ known, to find a relationship between $\mathscr{F}$ and C_D. The question arises of how to choose the value for V in a logical way. It is clearly less than the 3 cm s^{-1} total wave celerity but to go further use must be made of the theoretical results for the instability wavenumbers in the downslope, l, and crossslope, k, directions. First, for the present case $\tan^{-1}l/k = 50°$. Secondly, the total wavenumber $(l^2 + k^2)^{1/2} = m$, must be small enough that the wavelength, $l = 2\pi h_v/m$ is large and in the range 2 to 5 cm. The only possible location in the instability diagrams of Swaters (2003) where these conditions are met is in the lower right-hand corner of his figures 7, 8 and 11, very close to the marginal stability curve. After trying several possibilities a value of $V = 1.3$ cm s^{-1} seemed to give good results, with $\mathscr{F} = 0.150$ and $C_D = 0.265$. Here, as best as can be judged from figures 7 and 8, $l = 0.33$ and $k = 0.28$. These values give a value for $\tan^{-1}l/k = 50°$ and $m = 0.433$. The final step uses the definition of $\mathscr{F} = (4\pi/T)(h_v/g')^{1/2}/tg\alpha$, to calculate

$h_v = 0.195$ cm for $T = 20$ s. Finally, $\lambda = 2.83$ cm. This value is in the lower range of the observed values but this may simply be because figures 7 and 8 of Swaters (2003) do not extend to smaller values of l and k so close to the marginal stability boundary. This possibility is corroborated by the comment in Baines (1995, page 49), "-the flow is unstable with disturbances of long wavelength growing most rapidly at marginal stability". Note also, that the Froude number of the stream $Fr = V/(g'h_v)^{1/2} = 0.93$ and is at the lower end of the range in which Cenedese *et al.* (2004) found roll waves in their more controlled experiments. As mentioned above in Swaters (2003), with these values of $\mathscr{F}$ and C_D in the expression for V, $\mathscr{F}^2$ is a factor of ten less than $2C_D$, thus justifying our initial assumption that ignored $\mathscr{F}$ in the expression for V. Finally, the theory was calculated for a Reynolds number, $Re = (g'h_v)^{1/2}h_v/\nu = 400$. The values given above result in a value of Re of 100; however, it seems unlikely that the results of the calculation will be much affected by this slightly smaller value of Re.

It is clear from the very indirect arguments used above to connect experiment and theory that there is a need for experiments in which the quantities of interest, V, g' and h_v, are measured directly. Experiments of the type presented by Lane-Serff & Baines (1998) and Cenedese *et al.* (2004), but with an extended source region, would seem to have the best chance of doing this with some accuracy.

Finally we note that topographic variations, e.g. submarine canyons, can contribute significantly to the downslope flow by channelling dense fluid within them (Baines & Condie 1998). The effect of a canyon has been introduced into the present investigations, under a wide range of flow parameters. The buoyancy of the bottom flow channelled in the canyon was found to be considerably larger than that of either the downslope flow or the Kelvin current. The bottom water characteristics were observed to be similar to those without the canyon, except that the existence of the canyon weakened eddies and the Ekman layer propagating towards the canyon.

In the natural flows modelled here bathymetry is likely to play an important role in the flow behaviour (e.g. there are a large number of wide canyons that extend from the shelf to depth in the Weddell Sea, for example). Also buoyancy fluxes at the surface are unlikely to be uniform both spatially and temporally. However, the simple geometry used in this investigation has allowed some basic features of the flow to be isolated, and provides a basis for further study.

Support by NSF Ocean Sciences Contract Number OCE-0080069 is gratefully acknowledged. Thanks are due to Dr Arnold Gordon for bringing this problem to our attention and encouraging us to apply for funding. The authors also wish to thank the Associate Editor and the reviewers for their helpful suggestions.

REFERENCES

Armi, L. 1986 The hydraulics of two flowing layers with different densities. *J. Fluid Mech.* **163**, 27–58.

Baines, P. G. 1995 *Topographic Effects in Stratified Flows.* Cambridge University Press.

Baines, P. & Condie, S. 1998 Observations and modelling of Antarctic downslope flows: a review. In *Ocean, Ice and Atmosphere: Interactions at the Antarctic Continental Margin.* Antarctic Research Series, vol. 75 (ed. S. Jacobs & R. Weiss), pp. 29–49. AGU, Washington, DC.

Bromwich, D., Liu, Z., Van Woert, M. L. & Rogers, A. N. 1998 Winter atmospheric forcing of the Ross Sea polyna, In *Ocean, Ice and Atmosphere: Interactions at the Antarctic Continental Margin.* Antarctic Research Series, vol. 75 (ed. S. Jacobs & R. Weiss), pp. 101–134. AGU, Washington, DC.

Cenedese, C., Whitehead, J. A., Ascarelli, T. A. & Ohiwa, M. 2004 A dense current flowing down a sloping bottom in a rotating fluid. *J. Phys. Oceanogr.* **34**, 188–203.

Condie, S. 1995 Descent of dense water masses along continental slopes. *J. Mar. Res.* **53**, 897–928.

Cui, A. & Street, R. L. 2001 Large-eddy simulation of turbulent rotating convective flow development. *J. Fluid Mech.* **447**, 53–84.

Etling, D. F., Schrader, U., Brennecke, F., Kuhn, G., Chabert d'Hieres, G. & Didelle, H. 2000 Experiments with density current on a sloping bottom on a rotating fluid. *Dyn. Atmos. Oceans* **31**, 139–164.

Farmer, D. M. & Armi, L. 1986 Maximal two-layer exchange over a sill and through the combination of a sill and contraction with baratropic flow. *J. Fluid Mech.* **164**, 53–76.

Finnegan, T. D. & Ivey, G. N. 1999 Submaximal exchange between a convectively forced basin and a large reservoir. *J. Fluid Mech.* **378**, 357–378.

Gascard, J. C. 1991 Open ocean convection and deep water formation revised in the Mediterranean, Labrador, Greenland and Weddell Seas. In *Deep Convection and Deep Water Formation in the Oceans* (ed. P. C. Chu & J. C. Gascard), pp. 157–181. Elsevier.

Gill, A. E. 1973 Circulation and bottom water production in the Weddell Sea. *Deep Sea Res.* **20**, 111–140.

Gordon, A. 1998 Western Weddell Sea thermohaline stratification. Antarctic Research Series, vol. 75. AGU, Washington, DC.

Gordon, A. L., Huber, B., Hellmer, H. & Flied, A. 1993 Deep and bottom water of the Weddell Sea's Western rim. *Science* **262**, 95–97.

Griffiths, R. W. & Hopfinger, E. J. 1983 Gravity currents moving along a lateral boundary in a rotating fluid. *J. Fluid Mech.* **134**, 357–399.

Grimm, T. H. & Maxworthy, T. 1999 Buoyancy-driven mean flow in a long channel with a hydraulically constrained exit condition. *J. Fluid Mech.* **398**, 155–180.

Jacobs, P. & Ivey, G. 1998 The influence of rotation on shelf convection. *J. Fluid Mech.* **369**, 23–48.

Jet Propulsion Laboratory Images 1994 http://southport.jpl.nasa.gov/polar/sarimages.html.

Jones, H. & Marshall, J. 1993 Convection with rotation in a neutral ocean: a study of deep ocean convection. *J. Phys. Oceanogr.* **23**, 1009–1039.

Lane-Serff, G. & Baines, P. 1998 Eddy formation by dense flows on slopes in a rotating fluid. *J. Fluid Mech.* **363**, 229–252.

Lawrence, G. A. 1990 On the hydraulics of Boussinesq and non-Boussinesq two-layer flows. *J. Fluid Mech.* **215**, 457–480.

Maxworthy, T. 1996 A frictionally and hydraulically contrained model of the convectively driven mean flow in partially enclosed seas. *Deap Sea Res.* **44**, 1339–1354.

Maxworthy, T. 1997 Convection into domains with open boundaries. *Annu. Rev. Fluid Mech.* **29**, 327–371.

Maxworthy, T. 2002 Experiments on convection over a combined shelf and sloping bottom: bottom water formation at a continental margin. *USC Rep. January 2002.*

Maxworthy, T. & Narimousa, S. 1994 Unsteady turbulent convection into a homogeneous, rotating fluid, with oceanographic applications. *J. Phys. Oceanogr.* **24**, 865–887.

Mory, M., Stern, M. & Griffiths, R. 1987 Coherent baroclinic eddies on a sloping bottom. *J. Fluid Mech.* **183**, 45–62.

Muench, R. D. & Gordon, A. L. 1995 Circulation and transport of water along the Western Weddell Sea margin. *J. Geophys. Res.* **100**, 18503–18515.

Nagata, Y., Kimura, R., Honji, H., Kawaguchi, K. & Hosoyamada, T. 1993 Laboratory experiments of dense water descending on a continental shelf. In *Deep Ocean Circulation, Physical and Chemical Aspects* (ed. T. Teramoto), pp. 333–350. Elsevier.

Narimousa, S. 1997 Dynamics of mesoscale vortices generated by turbulent convection at large aspect ratios. *J. Geophys. Res.* **102 (C3)**, 5615–5624.

Nof, D. 1983 The translation of isolated cold eddies on a sloping bottom. *Deep-Sea Res.* **30**, 171–182.

Phillips, O. M. 1966 On turbulent convection currents and the circulation of the Red Sea. *Deep-Sea Res.* **13**, 1149–1160.

Swaters, G. E. 2003 Baroclinic characteristics of frictionally destabilized abyssal overflows. *J. Fluid Mech.* **489**, 349–379.

Whitworth III, T., Orsi, A. H., Kim, S.- J., Nowlin Jr, W. D. & Locarnini, A. N. 1998 Water mass and mixing near the Antactic slope front. In *Ocean, Ice and Atmosphere: Interactions at the Antarctic Continental Margin.* Antarctic Research Series, vol. 75 (ed. S. Jacobs & R. Weiss), pp. 1–28. AGU, Washington, DC.